High Surface Area Mesoporous Cotton Crop Biochar for Enhanced Confiscation of *p*-nitrophenol

Priyanka Doondani[1], Ajay Burile[2], Aman Bishnani[1], Ravin Jugade[1*]

[1]Department of Chemistry, RTM Nagpur University, Nagpur-440033, India

[2]Priyadarshini Bhagwati College of Engineering, Nagpur-440024, India

*Email: ravinj2001@yahoo.co.in

Received: 21.6.2024, Revised: 15.7.2024, Accepted: 20.7.2024

Abstract

This research study investigates the efficacy of utilizing biochar obtained from cotton crop residues for the enhanced remediation of *p*-nitrophenol (PNP). Cotton crop residue-derived biochar (CCB) was prepared using 1N phosphoric acid and subsequently characterized. Batch adsorption experimental analysis were conducted to assess the optimal adsorption capacity of CCB for PNP under various conditions, including temperature, pH, interaction time, initial PNP concentration, and dosage of biochar. The results demonstrated optimal adsorption capacity of 55.38 mg/g at pH 5.0, initial PNP concentration of 100 mg L^{-1}, and biochar dosage of 200 mg at a room temperature of 298 K. The experimental adsorption data exhibited an excellent correlation with the Redlich-Peterson isotherm model. Analysis of the sorption kinetics revealed that the material's uptake behavior closely followed a pseudo-second-order model. Thermodynamics analysis unveiled that the adsorption of PNP onto CCB was exothermic, spontaneous, and primarily driven by enthalpy. Overall, the findings suggest that CCB exhibits promising potential as an efficient adsorbent for the remediation of aquatic environments afflicted with presence of PNP.

Keywords: biochar; adsorption; p-nitrophenol; water treatment; organic pollutants.

1. Introduction

Water contamination has become a significant environmental concern, primarily due to the rapid expansion of industrial activities. Effluents discharged from industries such as petrochemicals, pesticides, and coking contain elevated levels of phenol, posing considerable challenges for treatment. The particular concern is the improper disposal of *p*-nitrophenol (PNP) by industries, given its role as an intermediate in the production of insecticides, pharmaceuticals, and other chemical compounds. Significantly, the presence of PNP with substituted hydroxyl (-OH) and nitro (-NO_2) groups is categorized as a highly hazardous contaminant, exerting adverse effects on the surrounding environment[1-3]. The adsorption method has attracted significant focus in contrast to alternative techniques for eliminating PNP, including membrane separation[4], extraction[5], biological methods[6] and advanced oxidation[7]. This preference is attributed to its perceived safety, operational simplicity, and capacity for reuse without causing secondary pollution[8]. Several adsorbents like activated Kaolinitic clay[9], HDTMA modified Natural Zeolite[10], $ZrSiO_4$-MnO_2 nanoparticles[11] and Montmorillonite[12] have been reported for the adsorption of PNP, but they often suffer from drawbacks such as low adsorption capacity, high cost, and complicated synthesis processes. Consequently, there is a pressing need to develop adsorbents that are both cost-effective and simple to synthesize for the efficient removal of PNP. In light of this, our research aims to address these issues by focusing on the development of such adsorbent for PNP removal. In recent years, we have reported various adsorbents for eliminating organic pollutants from water[13-17]; however, porous carbon material stands out as one of the most commonly utilized options. Its popularity stems from its extensive accessible surface area, well-established pore network, exceptional physical and chemical resilience, and diverse range of feedstock material sources[18]. Currently, porous carbon adsorbents are produced through several methods, encompassing thermal activation, chemical activation, and templating techniques. The thermal activation route involves gaseous substances like CO_2 or moisture in air as activation agents, followed by subsequent processing steps. However, this activation method necessitates elevated temperatures, typically ranging from 800 to 1000 degrees Celsius, resulting in substantial energy consumption[19,20]. Chemical activation is a valuable method for manufacturing porous carbon materials characterized to elevated specific surfaces and well-developed pore structures. Nevertheless, this process commonly employs corrosive alkaline or acidic activators such as NaOH, KOH, and H_3PO_4.

Biomasses, such as municipal solid waste (MSW), industrial organic waste, and agricultural residue[21], hold promising potential as natural adsorbents due to their abundant supply and cost-effectiveness[22,23]. Developing biochar-based sorbents is crucial for environmentally friendly sustainable development and efficient waste water treatment. Biochar, derived from thermal decomposition of biomass feed stocks at elevated temperatures, contains numerous oxygen functional groups (OFGs) and exhibits conductivity in water bodies. Furthermore, extensive research has been conducted on biochar's applications in soil. Combining environmental remediation, carbon sequestration, and affordable sorbents for pathogens and contaminants has garnered significant interest[10,24]. In the recent years, Zhang et al. utilized rapeseed and cabbage to produce layered double oxides and biochar for phosphate removal from aqueous solutions[25]. Similarly, Yi et al. developed an adsorbent from rice husk and wood chips using slow pyrolysis to enhance levofloxacin removal[26]. The results of these studies sparked our interest in synthesizing biochar. The combined research findings highlight biochar's multifaceted capacity as an efficient sorbent material for pollutant extraction.

The Vidarbha region in Central India, well-known for its cotton production, generates significant amounts of cotton straw as a byproduct. Unfortunately, much of this straw is discarded as waste. Recognizing activated carbon's high adsorptive potential due to its extensive surface area, our research was focused on producing biochar from waste cotton stalks. This study focuses on utilizing cotton crop residue-derived biochar (CCB) for the targeted removal of PNP, an organic toxicant.

2. Experimental

2.1. Chemicals

Adsorption experiments were conducted utilizing high-quality reagents and chemicals of analytical grade. *p*-nitrophenol was sourced from LOBA Chemie Pvt. Ltd., while phosphoric acid was procured from SRL, India. Deionized water was utilized for all experimental procedures. It's noteworthy that all the chemicals employed were of high purity, eliminating the need for additional refinement processes.

2.2. Synthesis of cotton crop residue derived biochar

The cotton crop residues underwent thorough cleaning to eliminate absorbed pollutants before being dried under sunlight and in a hot air oven to produce biochar. The synthesis of biochar was conducted following the procedure outlined in the literature with slight adjustments[27].

Subsequently, the dried residues were immersed in 1 N phosphoric acid for 24 hours. After treatment with phosphoric acid, the stalks underwent prolonged desiccation process in an hot air oven for extended period of 24 hours. It has now been proved that phosphoric acid treatment prior to pyrolysis leads to enhancement in surface area of biochar. This has been well-established fact that the change in surface area is attributed to crosslinking properties of phosphate ions[27]. Subsequently the dried material was subjected to pyrolysis in an electric muffle furnace. The pyrolysis was carried out at a high temperature of 600 °C for a time period of five hours, with continuous flow of nitrogen gas at a rate of 150 cubic centimeters per minute. After pyrolysis, biochar derived from cotton crop residues was obtained. This biochar was then mechanically ground to reduce its particle size to approximately 100 microns. The ground biochar was subjected to repeated rinsing with deionized water until the runoff exhibited neutral pH. This material was stored and labeled as cotton crop residue-derived CCB (CCB). Fig.1 illustrates the complete synthesis sequence for CCB.

2.3. Characterization methods

The synthesized CCB underwent comprehensive characterization using various analytical techniques. The surface morphology and structural features of CCB were examined through scanning electron microscopy (SEM), using TESCAN VEGA 3 SBH instrument. To investigate the crystalline nature, X-ray Diffraction (XRD) analysis was conducted using diffractometer system XPERT PRO Miniflex-300/600. This system operated at 300 W power with copper Kα radiation, scanning 2θ range from 1 to 100°. Chemical bond characteristics were investigated using Fourier-Transform Infrared (FT-IR) spectroscopy. A Bruker Alpha-E instrument, featuring a ZnSe attenuated total reflectance ATR crystal, analyzed samples across frequencies from 500 to 4000 cm^{-1}. The specific surface area (SSA) and porosity were evaluated by nitrogen adsorption-desorption measurements on a Quantachrome Nova 2200e BET surface area analyzer. The thermal stability of the synthesized CCB was assessed using a Shimadzu DTG-60 Differential Thermal Analyzer (DTA-TG) under a nitrogen atmosphere, with thermograms noted up to 600°C. Optical measurements were made using UV-Visible spectroscopy, employing a Shimadzu UV-1900i double-beam spectrophotometer functioning across 200 to 900 nm. Solution pH measurements were conducted by means of Equiptronics EQ-615 pH meter.

2.4. Batch Adsorption

Batch adsorption trials were performed to assess the adsorption capability of the newly synthesized CCB. In these experiments, predetermined amount of CCB was introduced into 25 mL of PNP solution with a specific pH and concentration. The mixture was stirred with a magnetic stirrer for a set duration to allow equilibrium to be reached. Following the adsorption period, the mixture was made to undergo separation using Whatman grade 1 filter paper. The residual PNP in the filtrate was quantified using spectrophotometer at 317 nm. The quantity of PNP adsorbed onto the adsorbent (mg/g) was then estimated with the help of mathematical equation (1) presented below:

$$q_e = \frac{C_0 - C_e}{W} \times V \quad (1)$$

The percentage of PNP removal was evaluated using the formula,

$$\%\ Removal = \frac{C_0 - C_e}{C_0} \times 100 \quad (2)$$

Where C_0 represents the initial PNP concentration (mg L^{-1}), C_e stands for equilibrium PNP concentration (mg L^{-1}), W represents CCB weight in g, and V signifies PNP solution volume (L). To validate the reliability of the experimental data, batch adsorption trials were conducted three times independently. The final reported values in the study represent the mean value calculated from the results of these three replicate experiments.

3. Results and discussion

3.1. Characterization

FT-IR spectroscopy can be utilized as an analytical technique to examine the nature of the interactions occurring between the adsorbent material and the p-nitrophenol (PNP) molecules during the adsorption process. The FTIR spectrum exhibited distinct absorption peaks at wave numbers 1577.02 cm^{-1} and 1698.73 cm^{-1}, which can be assigned to the stretching vibrational modes of aromatic C=C and C=O respectively. Additionally, the peaks detected at 1415.68 cm^{-1}, 1197.21 cm^{-1}, and 1160.28 cm^{-1} are indicative of the presence of C-O bonds characteristic of carboxylic acid moieties. The synthesized CCB showed aromatic groups and functional groups rich in oxygen which provide binding sites for the organic pollutant, PNP. Fig.2 represents the FT-IR spectra of the synthesized CCB.

SEM reveals the surface morphology of the CCB. Fig.3 represents SEM images at three different magnifications. SEM analysis of CCB revealed a textured surface morphology

characterized by numerous pores and folded regions. This unique feature, with its high degree of porosity and increased surface roughness, results in an augmented overall surface area for CCB. Consequently, the expanded surface area served to enhance the adsorption capacity of the CCB, enabling more efficient removal of target adsorbate species.

The assessment of surface area relies on the concept of single-layer adsorption-desorption of nitrogen molecules on the material's surface. Concurrently, the BJH technique employs the relationship between pore saturation pressures and nitrogen condensation within cavities to elucidate the pore size distribution of CCB. The CCB porosity characteristics and SSA were investigated through nitrogen sorption experiments, with the resulting equilibrium data as illustrated in[28] Fig.4a and 4b. Analysis indicated that the material possessed a considerable surface area of 405.7 m^2/g and a noteworthy pore volume of 2.4×10^{-1} cc/g. This remarkable increase in surface area can be linked to the presence of numerous microscopic voids within the material's structure. The mean pore width was calculated as 2.388 nm, indicative of its mesoporous nature. The equilibrium curve aligns with Type IV(a) in the IUPAC categorization system[29]. The BET equation parameter was determined to be 52.388, suggesting robust interactions between the adsorbate and the material's surface[30]. The synergy of substantial pore volume and expansive surface area significantly enhances the CCB exceptional capacity for toxicant capture[19].

Thermal stability of synthesized CCB was assessed using TGA-DTA analysis, which provides insights into the material's performance under various thermal conditions. The TGA analysis was conducted by ramping temperature at a controlled rate of 20 ℃ per minute while maintaining inert nitrogen environment with a continuous flow rate of 100 mL min^{-1}. The TGA curve for CCB revealed a total weight loss of 30% (Fig.4c), indicating good thermal stability. The DTA curve (Fig.4d) showed an endothermic peak corresponding to a weight loss of approximately 2% at 100 ℃. This observed reduction in weight results from the release of physically bound water molecule and atmospheric moisture from the CCB around 100 ℃. Additionally, the XRD analysis of CCB revealed the presence of well-defined peaks at 2θ = 25.12° and 46.02°, which are characteristic of biochar (Fig.4d). The peaks may be due to cellulose present in cotton crop. The XRD pattern shows that CCB is amorphous in nature.

3.2. Analysis of PNP adsorption studies on CCB

3.2.1. pH zero-point charge (pH_{zpc})

The adsorption behavior of molecule on a surface can be influenced based on the pH relative to the zero-point charge (pH_{zpc}). When the solution pH is below the pH_{zpc} value, the adsorbent acquires a positive surface charge, whereas above the pH_{zpc}, its surface becomes negatively charged[31]. Adsorption occurs for species with a charge opposite to that of the adsorbent surface. To experimentally determine the pH_{zpc} of CCB, a batch equilibration technique was conducted. This involved preparing nine separate mixtures, each containing 25 mL of 0.1 M NaCl solution with initial pH adjusted from 2.0 to 10.0, adjusted using HCl and NaOH. To each mixture, 100 mg of CCB was introduced, and the suspensions were continuously agitated for 24 hours using magnetic stirrers. Subsequently, the final pH of the filtrates was measured for each mixture. By plotting the change in ΔpH ($pH_{initial} - pH_{final}$) against the corresponding initial pH values, the pH_{zpc} for the CCB was revealed to be pH 7.8 (Fig.5a).

3.2.2. Effect of solution pH on PNP adsorption

The pH significantly influences the adsorption of PNP. To investigate this effect, a series of experiments were conducted. Seven beakers were prepared, each containing 25 mL of a 100 mg L^{-1} PNP solution with pH values spanning from 3.0 to 9.0, adjusted using appropriate acid or base solutions. To each beaker, 100 mg of the CCB was introduced, and the mixtures were continuously agitated for time period of 60 minutes to allow the adsorption process to occur. Following the agitation phase, the mixtures was subjected to separation, and the residual PNP in the filtrate was quantified. The findings indicated that PNP sorption by CCB reached its peak at pH 5.0, as depicted in Fig.5b. As the solution becomes more alkaline, the CCB's surface accumulates negative charges, resulting in electrostatic repulsion between the negatively charged PNP entities and the CCB surface. This interaction diminishes the CCB's-PNP capturing capacity.

3.2.3. Effect of CCB dosage on PNP adsorption

The effect of CCB dosage on PNP sorption was examined by varying the CCB amount from 10 to 400 mg in a 100 mg L^{-1} PNP solution maintained at pH 5.0. As illustrated in Fig.5c, the PNP-capturing efficiency enhanced with increasing CCB quantity, showing maxima at 200 mg. Subsequent additions yielded no further improvement. This saturation point is explained by the exhaustion of available PNP molecules at the given concentration. The findings indicate

that equilibrium was reached using 200 mg of the CCB, with additional amounts providing negligible benefits to the sorption process. Based on these observations, 200 mg was identified as the ideal quantity for subsequent sorption experiments.

3.2.4. Effect of interaction time

The influence of interaction time was assessed by altering the exposure time from 10 to 180 minutes for a 100 mg L^{-1} PNP solution (pH 5.0) with 100 mg of the CCB. The results are depicted in Fig.5d. Peak sorption occurred with 60 minutes of interaction time, at which point equilibrium was achieved[32]. Consequently, 60 minutes was determined to be the ideal interaction time for subsequent experiments.

3.2.5. Effect of initial PNP concentration

To determine the sorption capacity of CCB, 25 mL of PNP solutions with varying concentrations from 10 to 300 mg L^{-1} of pH 5.0 were prepared in individual beakers. Each beaker received 50 mg of CCB, and the mixtures were agitated continuously for 60 minutes. After agitation, the solutions were filtered, and the % removal of PNP was assessed. It was observed that the % removal was approximately 60% for concentrations up till 100 mg L^{-1}, but it decreased as the PNP concentration increased further. This trend is expected because higher PNP concentrations lead to fewer available adsorption sites on the adsorbent[33]. Therefore, a 100 mg L^{-1} concentration of PNP was selected for further investigations (Fig.5e).

3.3. Adsorption isotherms

Isotherm analysis were conducted to investigate sorption behavior of PNP onto CCB surface. These experiments involved varying the initial PNP concentration levels from 10 to 300 mg L^{-1} at pH 5.0, using 50 mg CCB dose, at 298 K for 60 minutes. The resulting data was analyzed utilizing various isotherm models, as presented in Table 1. The regression coefficient for both Langmuir and Redlich-Peterson (R-P) isotherm models were found to be very close to 1.0, suggesting the potential formation of a PNP monolayer on the homogeneous CCB surface[34]. (Fig.6a displays the best fitted isotherm model curve). Also, it can be observed from Table 1, that the χ^2 value for R-P isotherm is low, affirming that R-P isotherm is followed. The value of R_L= 0.034, being less than one, indicating favorable adsorption conditions. Furthermore, the Freundlich isotherm model parameter n = 3.462 suggests chemisorption process[35]. Additionally, the positive value of Temkin isotherm constant b = 299.2 J mol^{-1} signifies that

the adsorption process is exothermic[36,37]. The Redlich-Peterson model, which incorporates elements from both Langmuir and Freundlich isotherms approaches, provided the most accurate representation of the experimental results, suggesting that the process does not strictly adhere to ideal monolayer behavior[38].

The Table 1 compares the adsorption capacities of the synthesized CCB material with other adsorbents reported in literature for the removal of p-nitrophenol (PNP). As evident from the tabulated data, the CCB adsorbent demonstrates a remarkably high adsorption capacity towards PNP, outperforming various other adsorbent materials investigated for this application.

3.4. Adsorption kinetics

Adsorption kinetics provides insight into the rate at which the adsorption process progresses as a function of contact time (Fig. 7). The pseudo-first-order (PFO) kinetic model describes the rate of adsorption using the following rate expression[42]:

$$\log(q_e - q_t) = \log q_e - \left(\frac{k_1 t}{2.303}\right) \quad (3)$$

Where q_e(mg g^{-1}) is the amount of adsorbate adsorbed at equilibrium, q_t (mg g^{-1}) is the amount adsorbed at time t, the amount of PNP adsorbed at a certain time t and k_1(min^{-1}) is the PFO rate constant.

The pseudo-second-order (PSO) kinetic model, on the other hand, employs the following rate equation[43]:

$$\frac{t}{q_t} = \frac{1}{k_2 q_e^2} + \frac{t}{q_e} \quad (4)$$

Where k_2(g mg^{-1} min^{-1}) represents the PSO rate constant. Analysis of the correlation coefficients (R^2) revealed that the PSO model provided the best fit to the experimental kinetic data (Table 3). Additionally, the intraparticle diffusion (IPD) model suggested that pore diffusion is the rate-limiting step, as adsorbate ions can potentially diffuse into the adsorbent pores facilitated by magnetic stirring[44]. In the Weber Morris IPD model, the rate-determining step involves permeation of PNP from the bulk liquid phase to the solid surface of CCB. The rate expression for this model is as:

$$q_{t=} k_{int}.\, t^{1/2} + C \quad (5)$$

Where k_{int} (mg g^{-1} min^{-1}) denotes the intraparticle diffusion rate constant, and C is a constant related to the boundary layer effect. The non-zero intercept obtained from the plot (Fig. 7c)

indicates that both the diffusion process and the boundary layer play crucial roles in the rate-determining step[45]. Furthermore, the kinetic profile exhibits two distinct linear regions, suggesting an initial rapid diffusion phase followed by a gradual approach to equilibrium after 60 minutes. This is in agreement with various studies reported in literature[46].

3.5. Adsorption thermodynamics

The effect of temperature on PNP adsorption was investigated at different temperatures, specifically varying from 301 K to 316 K, using a temperature-controlled magnetic stirrer. Fig.5f indicates that temperature has a minor effect on the percentage removal. By examining the impact of temperature, it is possible to calculate various thermodynamic parameters. These parameters are essential for understanding the spontaneity and driving forces of the adsorption process.

The change in Gibbs free energy (ΔG) for the PNP adsorption process was calculated from the equilibrium constant K with the help of following equation (6):

$$\Delta G^\circ = -RT \ln K \quad (6)$$

The vant Hoff equation gives a relation between change in enthalpy (ΔH) and change in entropy (ΔS) by equation (7):

$$\ln K = \frac{\Delta S^\circ}{R} - \frac{\Delta H^\circ}{RT} \quad (7)$$

In these equations, R represents universal gas constant, T is the absolute temperature (K), ΔH is enthalpy change (kJ mol^{-1}), ΔG is Gibbs free energy change (kJ mol^{-1}), ΔS is entropy change (J mol^{-1} K^{-1}) and K is the equilibrium constant derived from the ratio of the amount of PNP adsorbed at equilibrium to the equilibrium PNP concentration in the liquid phase. The van't Hoff plot (Fig. 7d) provides the values for ΔH and ΔS, as listed in Table 4. The negative Gibbs free energy change indicates the spontaneity of the process. Additionally, the negative enthalpy change confirms that the process is exothermic, while the negative entropy change suggests a reduction in disorder during the adsorption activity. Given that the change in enthalpy is significantly more negative compared to TΔS, it can be concluded that this adsorption process is predominantly driven by enthalpy[31].

4. Conclusion

The cotton crop residue derived CCB was effectively synthesized by phosphoric acid treatment method. BET surface analysis characterization of the material revealed that the CCB has a mesoporous surface with a high pore volume and a surface area of 405.7 m²/g. This

composite serves as an excellent adsorbent, demonstrating an adsorption capacity of 55.38 mg of PNP per gram of CCB. The exceptional adsorption capacity arises from the CCB's high surface area and strong CCB-PNP interactions. Adsorption isotherm studies indicated that Redlich-Peterson isotherm model was followed. The thermodynamic evaluation affirmed the spontaneous nature of the adsorption process, governed predominantly by enthalpic contributions, while kinetic investigations suggested that the rate of adsorption adheres to a pseudo-second-order kinetic model. The produced material is cost-effective, environmentally friendly, and an efficient adsorbent for removing the organic pollutant PNP from industrial waste water. This research presents a novel approach, highlighting the potential application of CCB in water purification efforts.

Acknowledgements

Facilities provided by RTM Nagpur University are gratefully acknowledged. We are thankful to DST and UGC for funding under DST-FIST and UGC-SAP programs.

Figures:

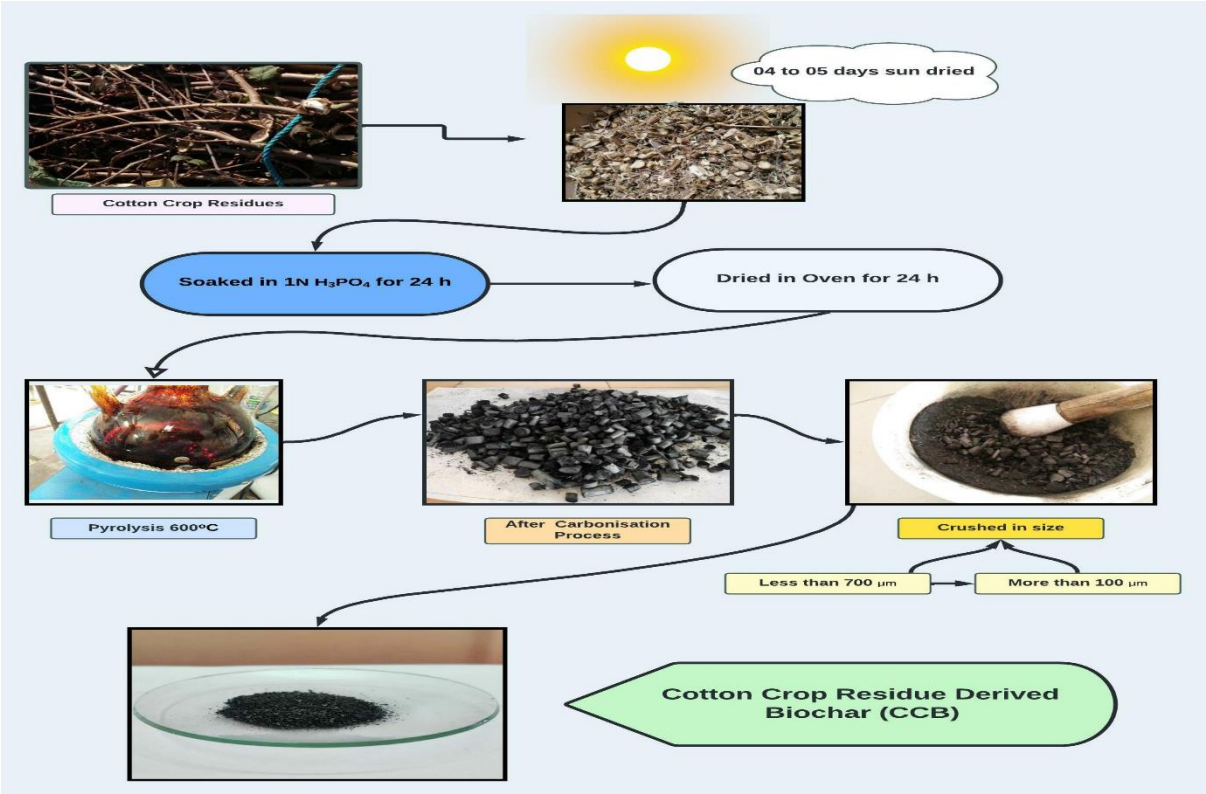

Fig. 1: Process flow diagram for synthesis of Cotton Crop Biochar (CCB)

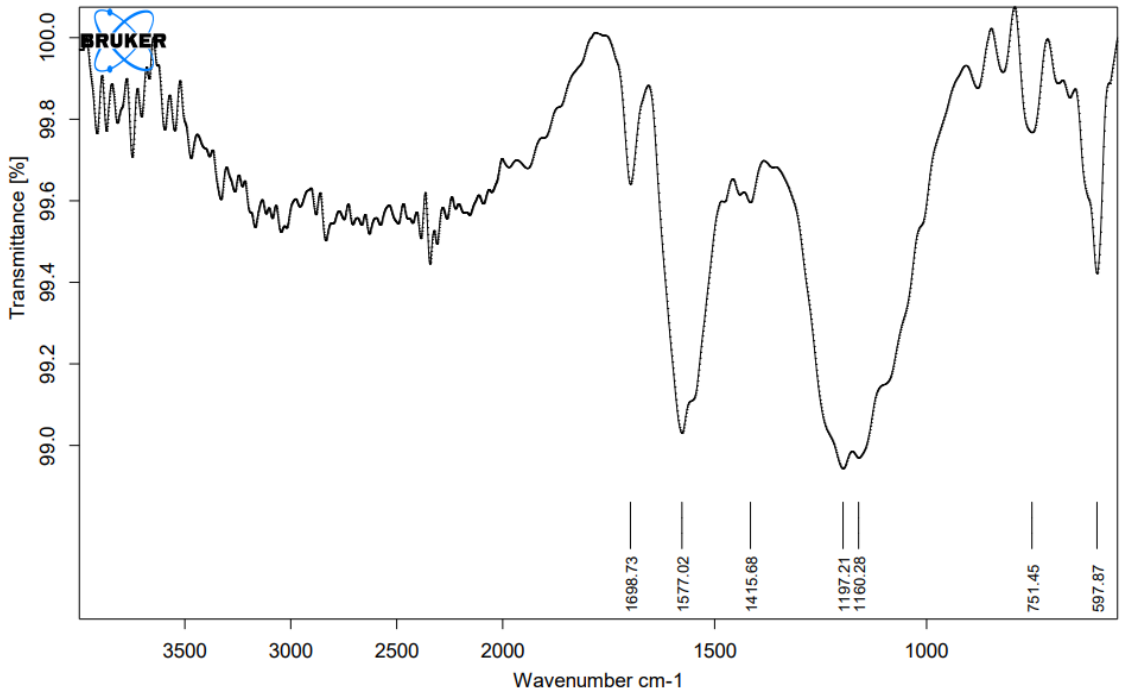

Fig. 2: FT-IR spectrum of CCB

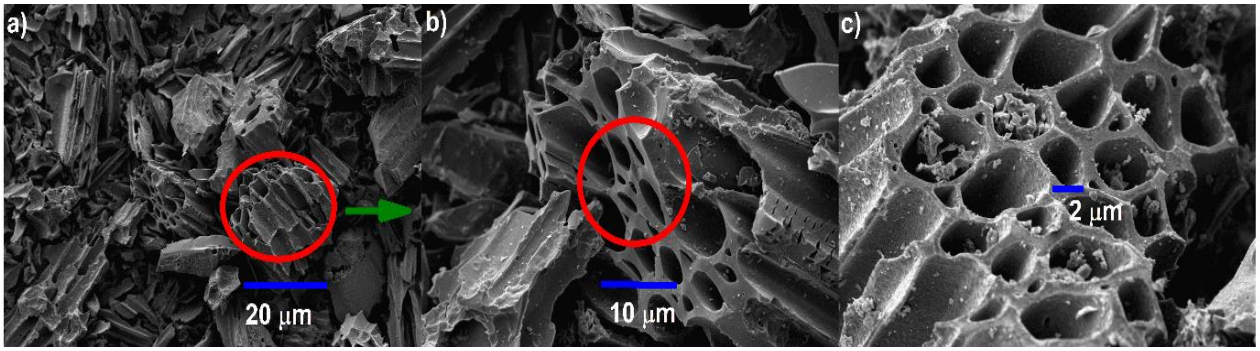

Fig. 3: SEM micrographs of CCB at three varying magnification levels a) 20 µm b) 10 µm c) 2 µm.

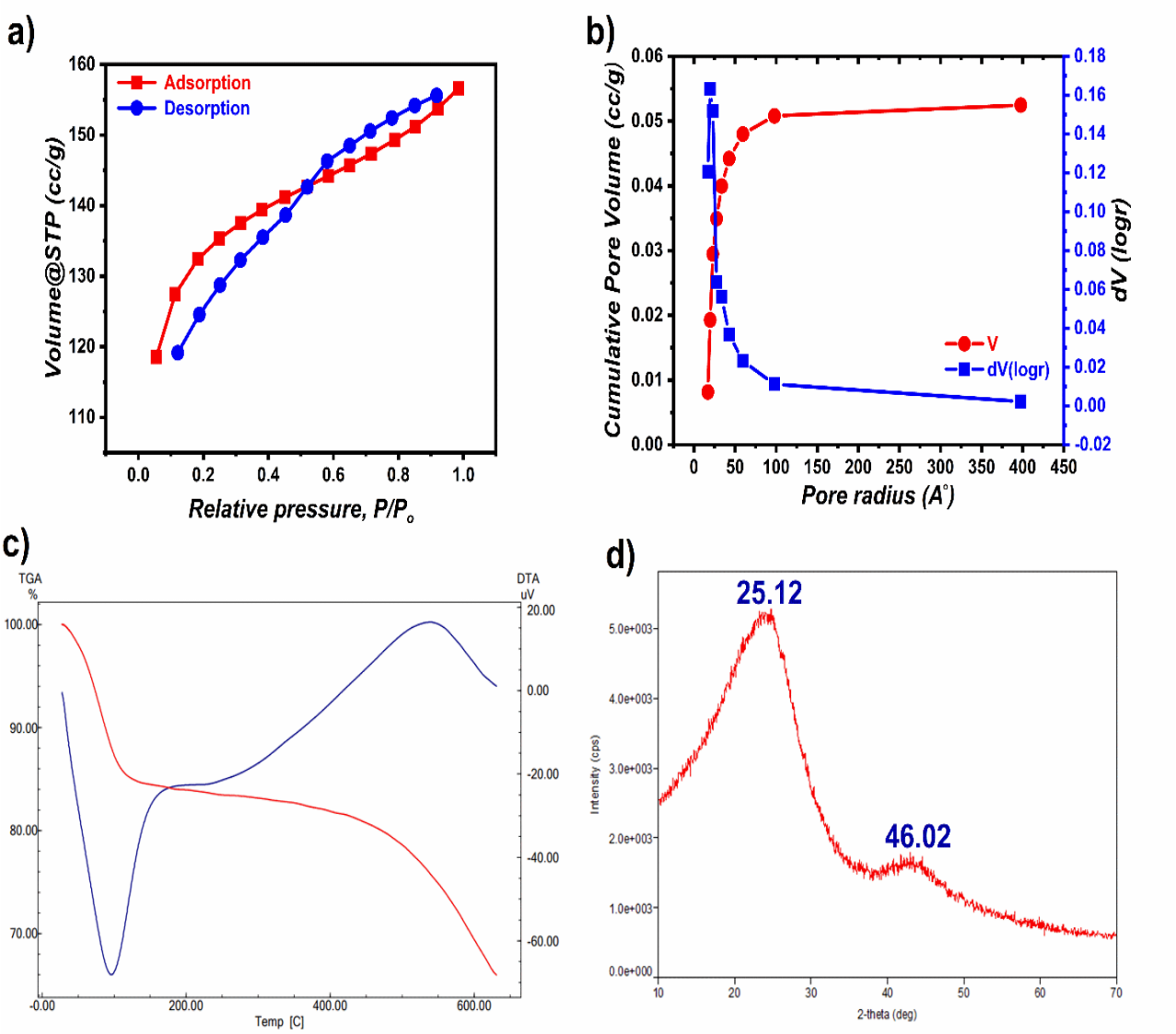

Fig. 4: a) Nitrogen sorption isotherm for CCB b) pore dimension distribution profile of CCB c) TGA-DTA analysis graphs of CCB d) XRD spectrum of CCB

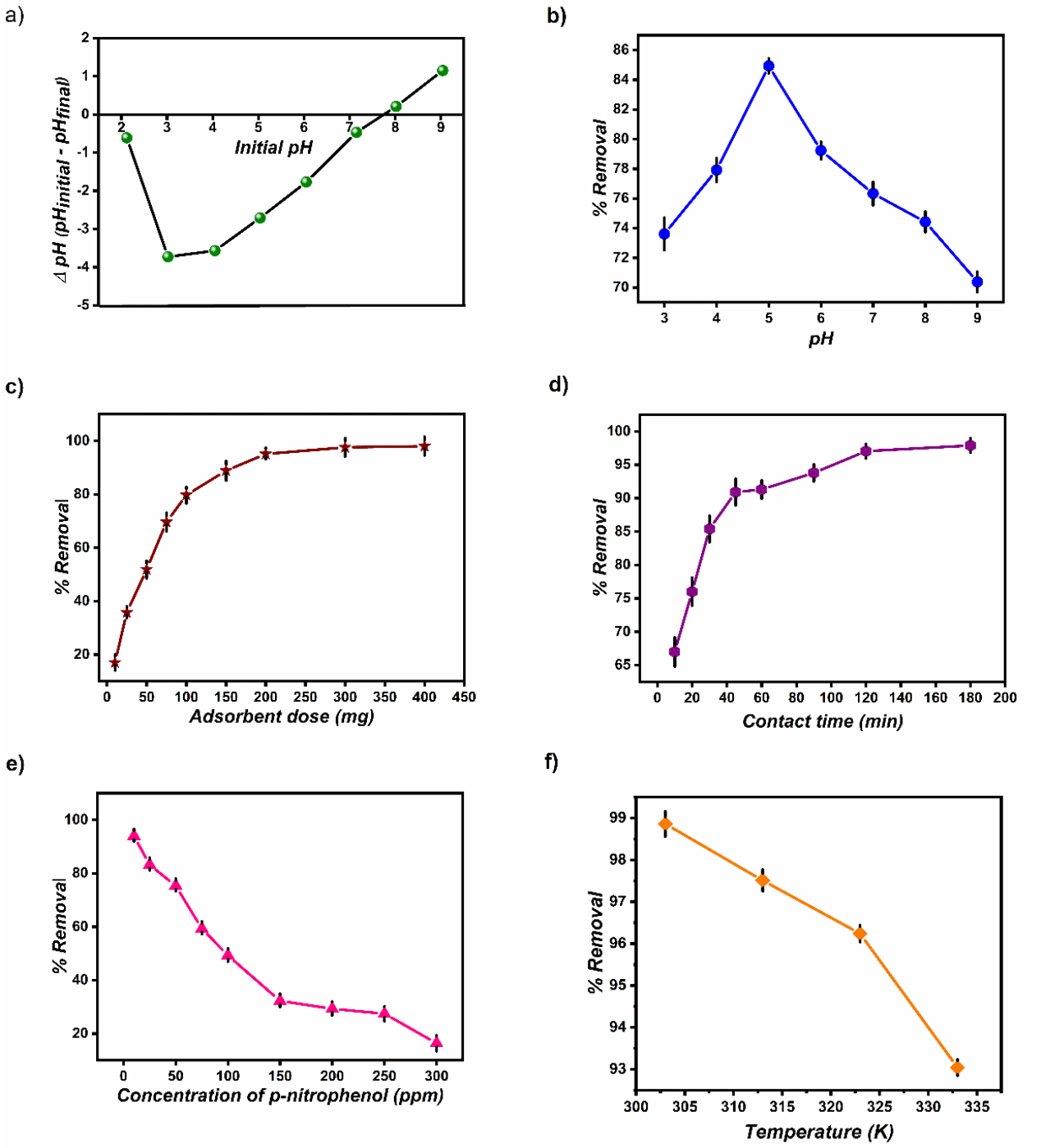

Fig. 5: a) pH_{zpc} curve of CCB b) effect of solution pH on PNP adsorption c) effect of CCB dosage on PNP adsorption d) effect of interaction time and e) effect of initial PNP concentration f) effect of temperature

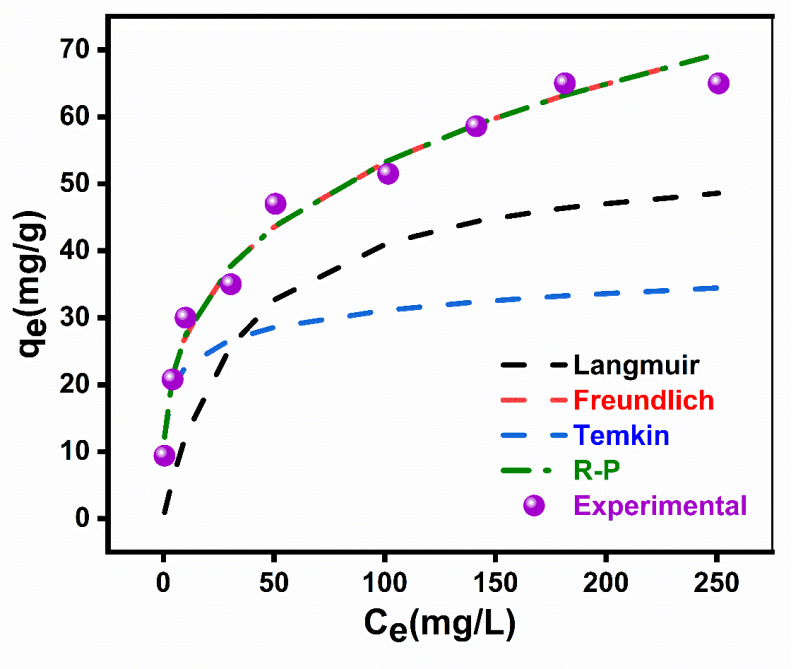

Fig. 6: C_e-q_e curves for comparative analysis of different isotherm models and experimental values for PNP adsorption onto CCB.

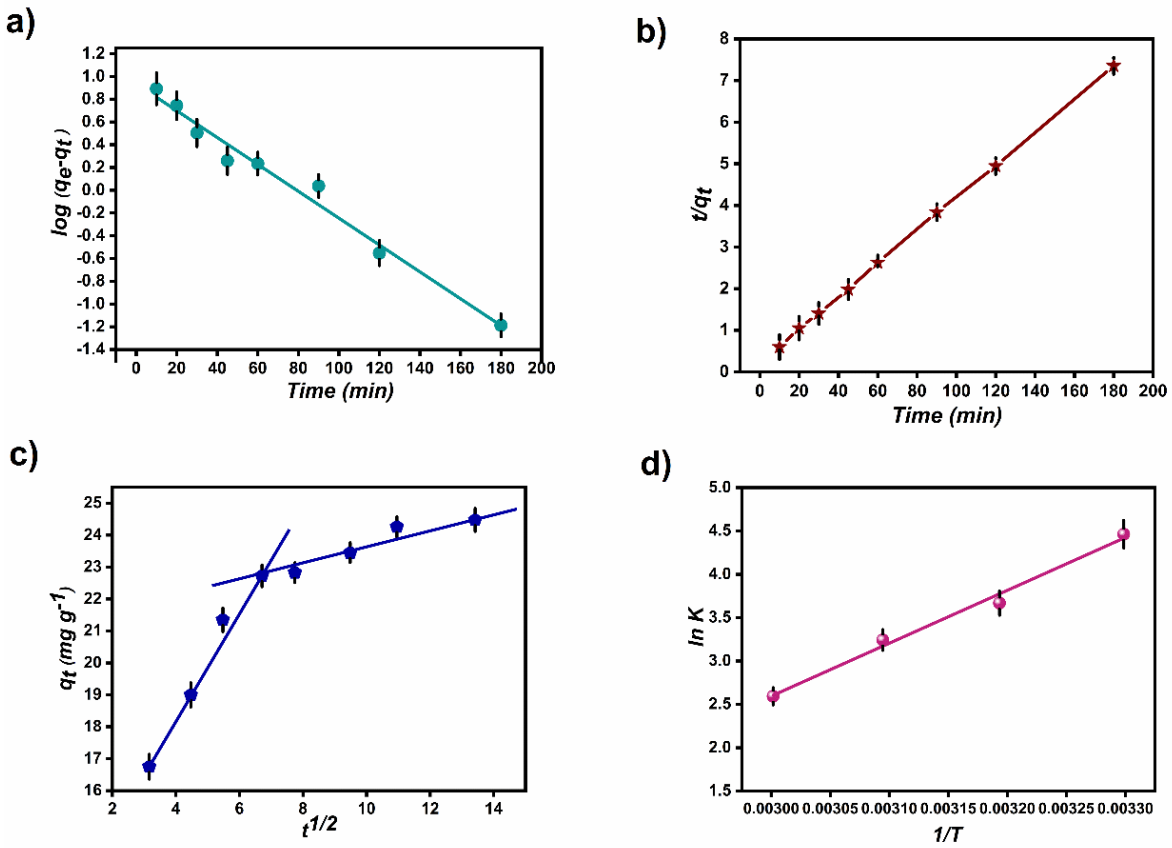

Fig. 7: (a) PFO plot, (b) PSO plot, and (c) IPD model plot (d) van't Hoff plot

Tables:

Table 1: Isotherm modeling parameters for adsorption of PNP onto CCB.

Model	Mathematical Parameters	Obtained values
Langmuir	q_m (mg g^{-1})	55.38
	b (L g^{-1})	0.282
	R_L	0.034
	R^2	0.961
	χ^2	1810.1
Freundlich	K_F ($mg^{1-1/n}$ g^{-1} L^{-1})	14.07
	N	3.462
	R^2	0.875
	χ^2	59.32
Temkin	b (J mol^{-1})	299.2
	A_T (L g^{-1})	5.436
	R^2	0.867
	χ^2	3510.5
Redlich-Peterson	b	0.711
	A	14.07
	R^2	0.977
	χ^2	59.32

Table 2: Comparison of highest PNP sorption capacities (q_m) onto various adsorbents at different pH values, along with the best-fit isotherm models.

Adsorbent	pH	Isotherm followed	q_m (mg/g)	References
Activated Kaolinitic clay	8.0	Freundlich	0.281	9
HDTMA modified Natural Zeolite	10.0	Langmuir	2.53	10
$ZrSiO_4$ -MnO_2 nanoparticles	4.0	Langmuir	12.09	11
Montmorillonite	3.0	Langmuir	15.30	12
Graphene	6.0	Langmuir	15.5	39
PDNH Nanocomposite hydrogel	7.0	Langmuir	19.20	40
CD@Si Composite materials	8.5	Freundlich	41.5	41
CCB	5.0	R-P	55.38	This study

Table 3: Kinetic parameters for PNP adsorption by CCB.

Kinetics model	Mathematical constants	Values obtained
PFO	k_1 (min^{-1})	0.0272
	R^2	0.9800
PSO	k_2 (g mg^{-1} min^{-1})	0.0073
	R^2	0.9990
IPD	k_i (mg g^{-1} $min^{-0.5}$)	0.6995
	C	16.4800
	R^2	0.7940

Table 4: Thermodynamic parameters

T(K)	ΔG (kJ mol^{-1})	ΔH (kJ mol^{-1})	ΔS (J mol^{-1} K^{-1})
303	-11.13	-50.72	-130.5
313	-9.825		
323	-8.519		
333	-7.213		

References

1. L. M. Cotoruelo, M. D. Marqu´es, F. J. Díaz, J. R. Mirasol, J. J. Rodríguez, and T. Cordero, *Chem. Eng. J.*, 184, 176, 2012.
2. G. Xue, M. Gao, Z. Gu, Z. Luo, and Z. Hu, *Chem. Eng. J.*, 218, 223, 2013.
3. Y. Zhou, X. Liu, L. Tang, F. Zhang, G. Zeng, X. Peng, L. Luo, Y. Deng, Y. Pang, and J. Zhang, *J. Hazard Mater.*, 333, 80, 2017.
4. W. Raza, J. Lee, N. Raza, Y. Luo, K.H. Kim, and J. Yang, *J. Ind. Eng. Chem.*, 71, 1, 2019.
5. B. Cui, J. C. Gong, M. H. Duan, Z. X. Chang, L. L. Su, W. J. Liu, and D. L. Li, *J. Chem. Eng. Data.*, 61(2), 813, 2016.
6. X. Zhang, Y. S. Yang, Y. Lu, Y. J. Wen, P. P. Li, and G. Zhang, *Water Res.*, 144, 616, 2018.
7. X. Dong, Z. Gan, X. Lu, W. Jin, Y. Yu, and M. Zhang, *Chem. Eng. J.*, 277, 30, 2015.
8. G. Wang, H. Xiao, J. Zhu, H. Zhao, K. Liu, S. Ma, S. Zhang, and S. Komarneni, *Environ. Res.* 201, 111496, 2021.
9. S. O. Azeez, and F. Adekola, *Pak. J. Anal. Environ. Chem.*, 17, 93, 2016.
10. J. Y. Guo, and B. Wang, *Huanjing Kexue Environ. Sci.*, 37, 1852, 2016.
11. M. E. Mahmoud, and G. M. Nabil, *J. Mol. Liq*., 240, 280, 2017.
12. M. Houari, B. Hamdi, O. Bouras, J. C. Bollinger, and M. Baudu, *Chem. Eng. J*., 255, 506, 2014.
13. P. Nandanwar, R. Jugade, V. Gomase, A. Shekhawat, A. Bambal, D. Saravanan, and S. Pandey, *J. Compos. Sci.*, 7, 103, 2023.
14. P. Doondani, R. Jugade, V. Gomase, A. Shekhawat, A. Bambal, and S. Pandey, *Water*, 14, 3411, 2022.
15. P. Doondani, V. Gomase, D. Saravanan, and R. Jugade, *Results Eng.*, 247, 100515, 2022.
16. P. Doondani, D. Panda, V. Gomase, K. R. Peta, and R. Jugade, *Environ. Res.*, 247, 118228, 2024.
17. P. Nandanwar, D. Saravanan, P. Bakshe, and R. Jugade, *Mater. Adv*., 3, 5488, 2022.
18. G. Singh, J. M. Lee, G. Kothandam, T. Palanisami, A. A. H. Al-Muhtaseb, A. Karakoti, J. Yi, N. Bolan, and A. Vinu, *Bull. Chem. Soc. Jpn*., 94(4), 1232, 2021.
19. S. Ahmed, J. Pan, M. Ashiq, D. Li, P. Tang, and Y. Feng, *Inorg. Chem. Front*., 6, 1952, 2019.

20. C.I. Contescu, S.P. Adhikari, N.C. Gallego, N.D. Evans, and B.E. Biss, *J. Carbon Res*., 4, 51, 2018.
21. W. Ding, X. Dong, I. M. Ime, B. Gao, and L. Q. Ma, *Chemosphere*, 105, 68, 2014.
22. M. B. Ahmed, J. L. Zhou, H. H. Ngo, and W. Guo, *Sci. Total Environ*., 532, 112, 2015.
23. D. Mohan, A. Sarswat, Y. S. Ok, and C. U. Pittman Jr., *Bioresour. Technol*., 160, 191, 2014.
24. T. Sizmur, T. Fresno, G. Akgul, H. Frost, and E. Moreno-Jimenez, *Bioresour. Technol*., 246, 34, 2017.
25. Z. Zhang, L. Yan, H. Yu, T. Yan, and X. Li, *Bioresour. Technol*., 284, 65, 2019.
26. S. Yi, B. Gao, Y. Sun, J. Wu, X. Shi, and B. X. Hu, *Chemosphere*, 150, 694, 2016.
27. G. Chu, J. Zhao, Y. Huang, and D. Zhou, *Env. Pollut*. 240, 1, 2018.
28. S. Brunauer, P. H. Emmett, and E. Teller, *J. Am. Chem. Soc*., 60, 309, 1938.
29. M. Thommes, K. Kaneko, A. Neimark, J. Olivier, F. Rodriguez-Reinoso, J. Rouquerol, and K. Sing, *Pure Appl. Chem.*, 87, 1051, 2015.
30. M. Thommes, B. Smarsly, M. Groenewolt, P. I. Ravikovitch, and A. V. Neimark, *Langmuir*, 22, 756, 2006.
31. S. Korde, S. Tandekar, and R. Jugade, *J. Env. Chem. Eng*., 8, 104360, 2020.
32. S. Kahu, D. Saravanan, and R. Jugade, *Water Sci. Technol*., 70, 2047, 2014.
33. S. H. Vithalkar, and R. M. Jugade, *Mater. Today: Proc.*, 29, 1025, 2020.
34. I. Langmuir, *J. Am. Chem. Soc*., 40, 1361, 1918.
35. H. Freundlich, *Z. Phys. Chem*., 57, 385, 1906.
36. O. Ferrandon, H. Bouabane, and M. Mazet, *J. Water Sci*., 8, 183, 1995.
37. G. Nechifor, D. Pascu, M. Neagu, G. A. Traistaru, P. C. Albu, *U.P.B. Sci. Bull., Series B*. 77, 1454, 2015.
38. N. Ayawei, A. N. Ebelegi, and D. Wankasi, *J. Chem*., 3039817, 2017.
39. A. I. Ismail, *Can. J. Chem*., 93, 1083, 2015.
40. M. T. Nakhjiri, G. B. Marandi, and M. Kurdtabar, *J. Environ. Chem. Eng*., 9, 105039, 2021.
41. H. M. Shen, G. Y. Zhu, W. B. Yu, H. K. Wu, H. B. Ji, H. X. Shi, Y. B. She, and Y. F. Zheng, *Appl. Surf. Sci.*, 356, 1155, 2015.
42. S. Lagergren, and K. Sven. *Vetensk. Handl*., 24, 1, 1898.
43. Y. S. Ho, and G. McKay, *Chem. Eng. J*., 70, 115, 1998.
44. W. Weber, and J. Morris, *J. Sanitary Eng. Div*., 89, 1, 1963.

45. A. Shekhawat, S. Kahu, D. Saravanan, and R. Jugade, *Int. J. Biol. Macromol*., 80, 615, 2015.
46. P. M. Nandanwar, S. H. Vithalkar, P. Bakshe, A. Shekhawat, and R. M. Jugade, *J. ISAS*, 1, 35, 2022.